A Comprehensive Tool for Modeling CMOS Image-Sensor-Noise Performance

Ryan D. Gow, David Renshaw, Keith Findlater, *Member, IEEE*, Lindsay Grant, Stuart J. McLeod, John Hart, and Robert L. Nicol

***Abstract*—Accurate modeling of image noise is important in understanding the relative contributions of multiple-noise mechanisms in the sensing, readout, and reconstruction phases of image formation. There is a lack of high-level image-sensor system modeling tools that enable engineers to see realistic visual effects of noise and change-specific design or process parameters to quickly see the resulting effects on image quality. This paper reports a comprehensive tool, written in MATLAB, for modeling noise in CMOS image sensors and showing the effect in images. The tool uses accepted theoretical/empirical noise models with parameters from measured process-data distributions. Output images from the tool are used to demonstrate the effectiveness of this approach in determining the effects of various noise sources on image quality.**

***Index Terms*—Image sensors, modeling, noise, simulation.**

I. Introduction

AN ACCURATE model of CMOS image-sensor-noise performance is useful in optimizing sensor design and setting targets, ultimately leading to improvements in image quality. Many attempts at modeling CMOS image-sensor noise are based on over-simplistic assumptions and may not incorporate a sufficient variety of noise sources to yield a realistic simulator [1]–[4]. Although noise can be quantified using various metrics, such as the signal-to-noise ratio (SNR), these are not necessarily a meaningful reflection of how camera users will perceive the image quality. These issues inspire the creation of a unified and accurate sensor-noise model capable of displaying noisy end-images. In this paper, we present such a tool.

First, CMOS image-sensor noise is introduced along with the general modeling approach used in this paper. Next, we discuss the techniques used to model each source of noise associated with charge collection. This includes photon shot noise, photoresponse nonuniformity (PRNU), crosstalk, and dark current [5]. Emphasis is given to the treatment of non-Gaussian random noise: Instead of simply assuming a Gaussian distribution for all random noise, we offer more representative distributions where appropriate. Then, the modeling of circuit noise is discussed. This includes column, row, low-frequency, thermal, and quantization noises. Finally, an overview of the complete tool is presented, and its usefulness is demonstrated with some sample applications.

Manuscript received August 16, 2006; revised December 13, 2006. This work was supported in part by STMicroelectronics and in part by the Scottish Funding Council for the Joint Research Institute with the Heriot–Watt University, which is a part of the Edinburgh Research Partnership. The review of this paper was arranged by Editor J. Tower.

R. D. Gow was with the University of Edinburgh, EH9 3JL Edinburgh, U.K., and STMicroelectronics, Edinburgh, U.K. He is now with the University of Cambridge, CB2 1TN Cambridge, U.K. (e-mail: ryan.gow@gmail.com).

D. Renshaw is with the Institute for Integrated Micro and Nano Systems, Joint Research Institute for Integrated Systems, School of Engineering and Electronics, The University of Edinburgh, EH9 3JL Edinburgh, U.K. (e-mail: david.renshaw@ee.ed.ac.uk).

K. Findlater was with STMicroelectronics, Edinburgh, U.K. He is now with Gigle Semiconductor, Edinburgh, U.K. (e-mail: keith.findlater@ieee.org).

L. Grant, S. J. McLeod, J. Hart, and R. L. Nicol are with STMicroelectronics, Edinburgh, U.K. (e-mail: lindsay.grant@st.com).

Digital Object Identifier 10.1109/TED.2007.896718

II. Noise Sources and Types

The imperfections or "errors" found in real images result from the optics, sensor, and color processing chain. In this paper, only artefacts associated with the CMOS sensor are considered. These may be in the form of fixed offsets or may be random noise, in which pixel values exhibit statistical variation with respect to time and/or location. Clearly, the temporal and time invariant components—known as fixed-pattern noise (FPN)—are indistinguishable if the system is sampled at only one instant in time, as in still images. Depending on its nature, the noise may also vary with temperature and signal level [2], [6], [7]. Our model accounts for these dependencies where necessary. Fig. 1 shows where the main noise sources occur in the pipeline of the four-transistor (4T) active pixel sensor on which this paper is based [8].

III. Perfect Images

To accurately evaluate the impact of noise on image quality, it is essential that the noise is added to initially noiseless images. Lifelike scenes are needed for evaluating the perceptual impact of noise in end-applications. Hence, we utilize ray-tracing software [9] to generate noiseless realistic scenes. In addition, photographs obtained using a very high-quality digital camera may provide a sufficiently high SNR to be considered "perfect" for practical purposes. The model is capable of handling monochrome and color images. For the latter, we assume that the sensor utilizes a Red-Green-Blue Bayer-patterned color filter array (CFA) [10].

Whichever image is selected for use in the model, its pixel values are normalized to represent electrons in the photodiode. This is determined by the user specifying the peak number of photo-generated electrons per second and the integration time and full-well capacity of the pixel. We, therefore, have the ability to control a wide variety of input scenes to which noise can be added in order to achieve a realistic image.

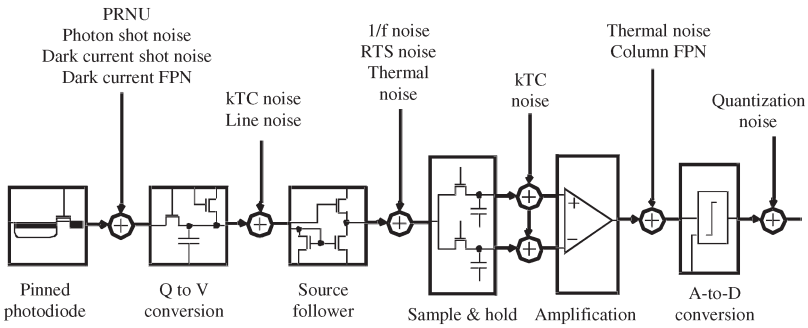

Fig. 1. Main noise sources in the CMOS imager pipeline (adapted from [5]). Note that photodiode kTC noise is not modeled in this paper as our model refers to 4T pixels, which allow the effect of this form of noise to be eliminated.

IV. Modeling Random Noise

An $m \times n$ noisy image for one type of random noise can generally be considered as $m \times n$ runs of a single random variable (rv). Several sources of random noise, therefore, can be modeled by superposing $m \times n$ realizations of appropriate stochastic processes. Each rv has a corresponding probability distribution function (pdf), which contains the most important information about the variable. Hence, modeling random noise in images entails using suitable probability distributions to generate matrices of noise values.

V. Charge Collection and Associated Noise

A. Photon-Shot-Noise Model

Due to the quantum nature of light, there is an inescapable uncertainty in the number of photons collected in the photodiode—this is termed photon shot noise. The number of photons incident in a given observation window is known to follow the Poisson distribution, with the variance equal to the mean arrival rate [11], [12]. Thus, photon shot noise can be simulated by reading each pixel value in the perfect input image and generating a random number using the Poisson distribution (or normal distribution for large pixel values > 1000 [13]), with the mean arrival rate equal to that pixel value. The resulting matrix represents the image incorporating photon shot noise.

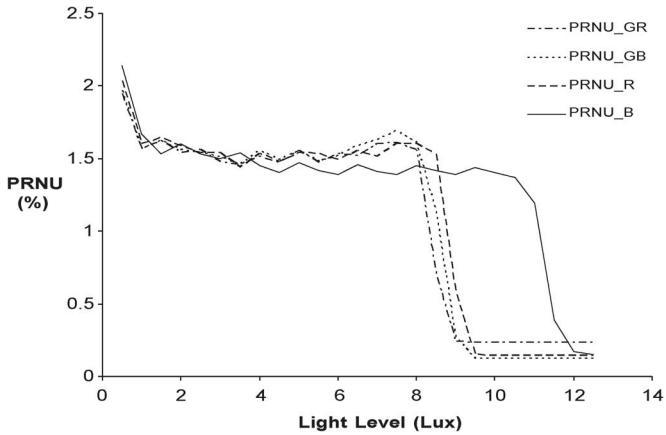

Fig. 2. PRNU at different light levels for a prototype sensor.

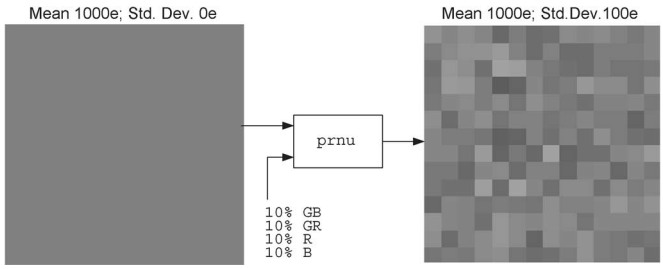

Fig. 3. Impact of PRNU on a flat-field gray scene (14 × 14 pixels).

B. PRNU Model

PRNU describes the fact that not all pixels have the same response to light due to process variations [2]. This is usually considered as a pixel gain-mismatch phenomenon, so PRNU is classed as a signal-dependent FPN. It is typically quoted as a percentage of the mean signal value. Fig. 2 demonstrates the signal-dependent nature of PRNU for a recent color-image sensor. This form of noise is becoming increasingly significant as the trend toward smaller pixels makes fabricating identical pixels ever more difficult [14].

In modeling PRNU, it is necessary to consider the variation in output pixel values across the image array. Thus, a histogram of pixel values from the difference frame used to measure PRNU was generated. By superposing a normal distribution with the same mean and standard deviation as the measured data, we were able to obtain a reasonable fit. Therefore, given that the normal distribution approximates the actual data reasonably well, this distribution was used in the model. A gain map is generated using a normal distribution with a mean of unity and a standard deviation equal to the measured PRNU. This gain map is then applied on a pixel-by-pixel basis to the input image. The gain map remains fixed over multiple frames.

The model is based on some assumptions. Notably, we ignore the signal dependence of the PRNU. Fig. 2 showed that the PRNU percentage variation with signal is approximately constant, except at extremely low or high light levels. It is, therefore, reasonable to treat the PRNU as being independent of signal. An example output is illustrated in Fig. 3, which shows the impact of 10% PRNU on an image of mean 1000 electrons.

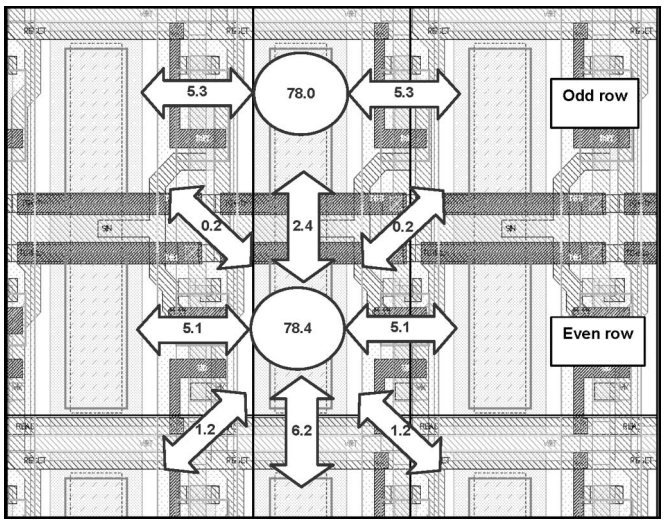

Fig. 4. Example measurement result for crosstalk under Green illumination.

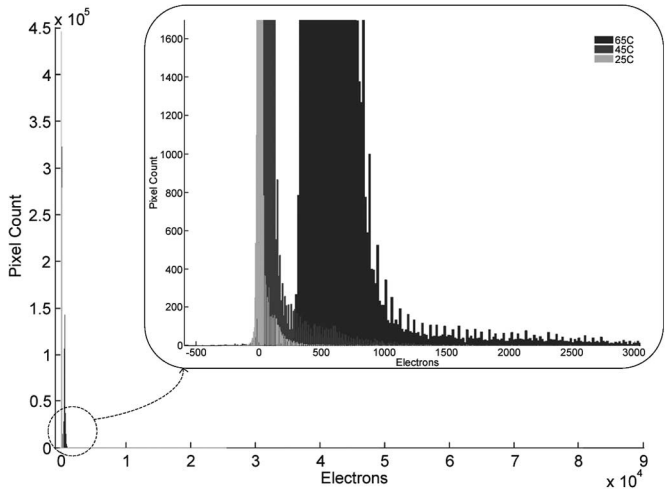

Fig. 5. Shifted and scaled histograms illustrating the dark-current distribution at different temperatures (for a sensor taken at 1-s exposure). Note that the shape, as well as the location of the distribution, varies with temperature.

C. Crosstalk Model

Crosstalk between pixels is caused by two different mechanisms: optical and diffusion crosstalks. Since our model does not aim to simulate optical effects, only the crosstalk due to diffusion in the sensor is considered. This phenomenon causes color mixing, image blur, and degrades the SNR after color reconstruction [15]. Like PRNU, crosstalk is becoming an increasingly significant problem, given the trend toward smaller pixel dimensions.

To evaluate diffusion crosstalk, a single pixel should be exposed to light, and the resulting values for that pixel and its neighbors—which are shielded from light by a metallization layer—must be measured. The signal measured in each neighboring pixel can then be expressed as a percentage of the total signal, thus providing a measure of the crosstalk in each direction. The results of such a characterization are shown in Fig. 4 for a pixel implemented in 0.18-μm CMOS image-sensor technology.

Given these parameters, it is possible to simulate crosstalk as follows. 1) Determine the proportion of original pixel value remaining after experiencing crosstalk (i.e., by scaling by 78.4% in the example above). 2) Then, add the crosstalk contribution from the surrounding pixels. The process is repeated for each pixel in the input image to generate a corresponding output image with crosstalk.

The crosstalk parameters are modeled as being constant for a given run of n frames resulting in scene-dependent crosstalk. It is assumed that the crosstalk is constant across the pixel array, which in reality will not be the case due to variation in chief ray angle, which changes the location of the photo generation inside the pixel. Furthermore, the model assumes that the number of crosstalk electrons is always linearly proportional to the pixel values. In reality, this may not be true, but real sensor data was unavailable to investigate this more thoroughly.

Crosstalk in sensors featuring a CFA results in color mixing between the channels. Hence, the color-reconstruction process (see Section IX) must compensate by applying an appropriate white balance and color matrix (details of which can be found elsewhere [16]–[18]).

VI. Dark Current

Dark-current generation centers are randomly distributed spatially in the silicon (Fig. 5). In other words, different pixels produce differing amounts of dark current, and this is termed the dark-current nonuniformity (DCNU). This manifests itself as a fixed-pattern exposure-dependent noise. There is also a temporal noise associated with it known as the dark-current shot noise (DCSN) [19]–[22].

The task of modeling dark current in images, therefore, requires generating DCNU arrays with realistic statistical properties and, then, given that the DCSN follows the Poisson distribution, applying a shot noise to each pixel.

A. Modeling DCNU

Some previously published attempts assume that the DCNU is Gaussian distributed [2], [3], but examination of sensor-characterization data shows that this is a flawed assumption. Indeed, from Fig. 6, it is clear that a tiny proportion of pixels in the array show extremely high levels of dark current. Such pixels will rapidly saturate, appearing as white dots in a low-light scene, which considerably degrades the perceived-image quality. Accounting for these "white" pixels is, therefore, of paramount importance, particularly as when two white pixels are adjacent in an image a couplet results, which is difficult to remove by signal processing. Couplets are a key driver in the manufacturing yield of high-volume image sensors [21].

Furthermore, the generation of dark current is highly temperature-dependent, doubling approximately every 6 °C–8 °C in crystalline silicon [20]. In order to reflect realistic operating conditions, characterization at multiple temperatures is needed (see Fig. 6). Very leaky pixels appear to have a lower temperature coefficient than less leaky pixels. This is likely due to different physical mechanisms behind the dark current [22].

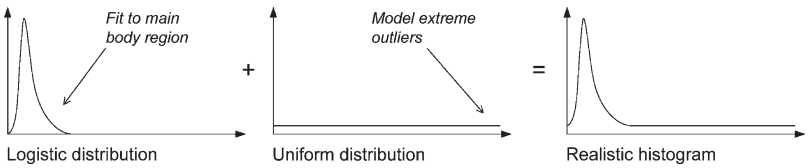

Fig. 6. Concept of using two distributions to achieve a more realistic end-histogram.

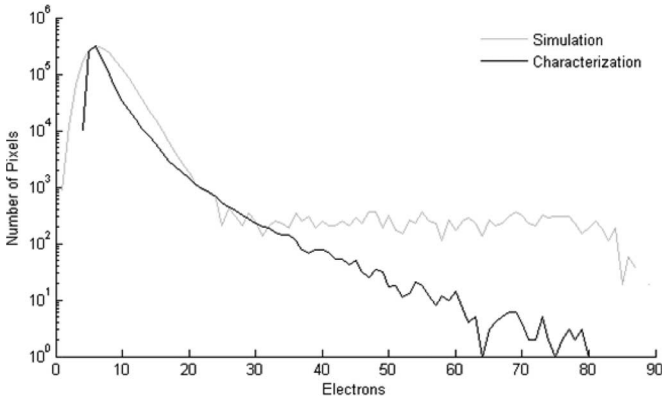

Fig. 7. Outline of a temporal noise distribution measured on a prototype sensor, and a fit to the real data using the FTG and uniform distributions.

1) Simulating DCNU at 25 °C: We initially sought to fit the entire dark-current histogram to one of the many available probability distributions. However, all of the "fits" were visibly poor. This is not surprising: Difficulty in accounting for both the extreme outliers, as well as accurately following the main body of the distribution, is undoubtedly the reason why some previous attempts have succumbed to using the normal distribution. In modeling the DCNU, we first propose a distribution for the main body region and account for the outliers separately.

When fitting a distribution to sample data, MATLAB returns the best fit parameters for that distribution and a log-likelihood value [23], [24]. Using this metric along with visual comparisons, the logistic distribution was selected to model the shape of the main body of the dark-current histogram at 25 °C. This distribution is an alternative to the normal distribution, where a higher proportion of the population is distributed in the tails [25].

It is now necessary to consider how to model the ultra noisy white pixels. From a histogram perspective, this means finding a method to extend the right-hand tail. Since one all-encompassing distribution could not be found, a superposition of the distributions was considered. The uniform distribution [13] was considered the most intuitive for this purpose, since its rectangular-shaped pdf can add to the logistic pdf, as shown in Fig. 7.

To avoid adding excessive noise to the main body, only a certain proportion of the uniformly distributed data must represent the high noise values and all other elements must be set to zero. In benchmarking sensors, an important metric is the parts per million (ppm) of pixels with the dark current greater than a given threshold, and we, therefore, incorporate this as an input parameter in the model. This technique was shown to produce realistic end-histograms.

2) Simulating DCNU at Other Temperatures: The DCNU at 45 °C and 65 °C was modeled using the same procedure as employed for 25 °C. However, we found that the inverse Gaussian [26] (also known as the Wald distribution) and log-normal [27] distributions were the best fits for the main body at these temperatures with a uniform distribution superimposed to model "white" pixels. Modeling performance at 25 °C, 45 °C, and 65 °C is adequate for most purposes, and the modular structure of our model allows for easy extension to other temperatures.

B. Modeling DCSN

Dark-current pixel values in any individual frame are affected by the associated shot-noise component. Therefore, to simulate an individual frame, it is necessary to apply shot noise to the DCNU array. This is exactly analogous to modeling photon shot noise on a perfect image array. Hence, we use the same algorithm as discussed in Section V-A.

VII. Pixel Circuit Noise

Noise present out with the photodiode depends on the circuit design and processing technology used. This includes thermal noise, flicker noise, random telegraph signal (RTS), row noise, and column noise. These types of noise are particularly important to model: Thermal noise sets the fundamental temporal noise floor, flicker and RTS are becoming increasingly significant as pixel dimensions shrink, and artefacts appearing as rows or columns in the image are particularly noticeable.

A. Modeling Thermal Noise

Thermal noise is present at the source follower, in the readout transistors, and in the analog-to-digital converter (ADC) of an imager. It is known to follow a zero-mean Gaussian distribution [20], so modeling thermal noise simply requires generating a normal distribution with appropriate standard deviation.

B. Modeling Flicker/RTS Noise

Low-frequency "flicker" noise (known as $1/f$) and RTS are crucial components of the source-follower noise. These are due to the action of traps in the silicon lattice which randomly capture and emit carriers [28]. This modulates the channel conductance, leading to a noise signal.

In analyzing the histogram of the temporal pixel noise for contemporary imagers, we observed that it appeared to have a "fat tailed" distribution. This is similar—but not nearly as extreme—as that observed with dark current, as detailed in

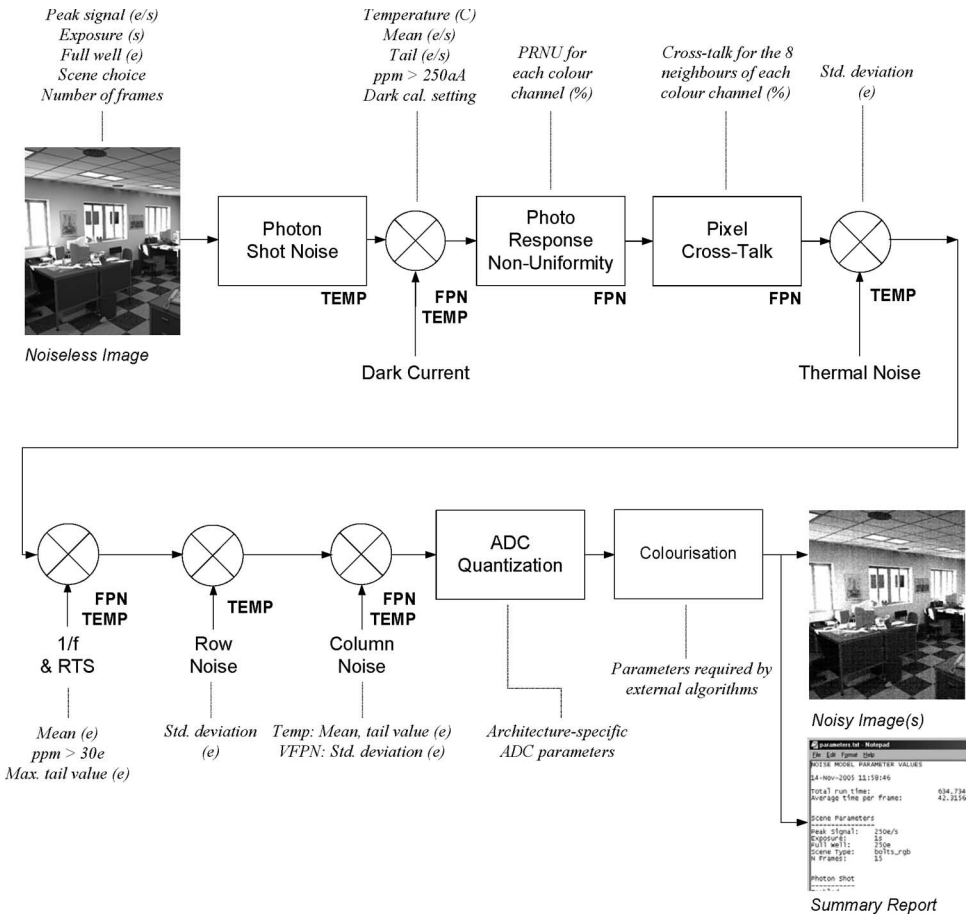

Fig. 8. Block diagram of the overall sensor-noise model.

Section VI of this paper. It is the extremely noisy pixels, which are most disturbing, that, in this case, manifest themselves as flickering dots in a video sequence. Since we know that the thermal component of pixel circuit noise is Gaussian distributed, completing the pixel-circuit-noise model thus requires finding a suitable distribution for the flicker and RTS components.

However, flicker and RTS are not fully understood phenomena, and the notion that flicker noise can be regarded as a superposition of single-carrier RTS has been debated in the literature [28]–[31]. No definitive understanding exists of how flicker noise or RTS values are distributed across an array of transistors. Nonetheless, a connection has been made between the fluctuation of flicker noise and the field of extreme value statistics. Specifically, it has been shown that voltage fluctuations in gallium arsenide (GaAs) films, which exhibit a $1/f$ power spectrum, following the Fisher–Tippet–Gumbel (FTG) distribution [32]–[35].

This inspired the use of the FTG distribution (also known as the log-Weibull or type-1 extreme value) to simulate the long tails of the flicker-noise histogram. We found that the FTG distribution could not yield a good fit to both the main body region of the histogram and the extreme tail values. Therefore, as when modeling dark current (see Section VI), we make use of a superposition with the uniform distribution. This enables us to obtain appropriate tail values. The resulting histogram represents the fact that different pixels have different levels of temporal noise when measured over many frames.

This technique provides a reasonably accurate method of modeling the characterization data, as shown in Fig. 8. Although the simulated data does not rolloff like the characterization data, the ppm count is the same—something which is in fact more important than the absolute value of the noise, since the differences are likely to be imperceptible in a typical image.

The distribution shown in Fig. 7 is the variation in random temporal noise across the array. It does not mean that the random temporal noise for a specific pixel varies in time according to such a distribution. However, since no definitive understanding could be found on the statistical properties of flicker and RTS per pixel, these components could not be separated and parameterized individually. Our model, therefore, assumes that the overall flicker/RTS in each pixel obeys a zero-mean normal distribution, with the standard deviation taken from the FTG/uniform distribution. This is a simplification of the real behavior. The normal distribution thus provides the necessary temporal variation, albeit through a simple assumption.

C. Modeling Row Noise

When a given row is released from reset, all pixels in that row are exposed to noise entering through the reset line, transfer

gate, or read transistor. This appears in images as horizontal lines and has fixed and temporal components. Normally, the fixed component can be neglected, as fixed offsets between color channels can be removed by subsequent color reconstruction. Hence, our model only considers the temporal row noise.

The distribution of row noise was measured and was found to follow a Gaussian distribution; therefore, it can be modeled by generating a random value per row and applying it to all the pixels in that row. As this noise is time varying, a new value is generated for each row in each frame to be simulated.

D. Modeling Column Noise

Noise appearing in vertical lines is also highly noticeable, although the mechanism is different to that of row noise. Our model is based on an in-column ADC architecture, and so, temporal column noise includes thermal and $1/f$ noise in the column amplifiers, although the biggest component is introduced by the sample and hold capacitors during reset. This is known as column-level "kTC" noise.

Vertical FPN (VFPN) is caused by mismatch between column amplifiers, leading to offset (signal-independent) and gain (signal-dependent) components. Through careful design and fabrication, differences in column gain can be reduced, which means that the offset component is more significant. Thus, the signal dependence may be neglected to a first order.

1) Temporal Column Noise: Our measurements revealed that the histogram of temporal column noise is right skewed, indicating that a few columns are much noisier than others, similarly to the pixel source-follower noise. It is, therefore, intuitive to consider applying the FTG distribution to model temporal column noise. By careful choice of input parameters, we were able to match the mean and also the outliers of the measured distribution rather well (no uniform-distribution addition was required). The simulation data is then generated in an algorithm similar to that used for temporal row noise, only the random data is arranged in columns and is derived from the FTG distribution.

2) Vertical FPN (VFPN): The fixed-pattern component of column noise is known to be more significant than the temporal component, and fixed vertical lines are easily perceptible in video sequences. Once more, examination of the histogram revealed that the distribution of VFPN was Gaussian. It was modeled by generating a single value per column of pixels in the array and adding each value to the pixels in that column. To create an FPN, the column values remain fixed over multiple frames.

VIII. Analog-to-Digital Conversion

It is now appropriate to move further through the imaging chain to consider the quantization noise introduced by the ADC. Our model is based on a column parallel ADC architecture [8], [36].

The digital ramp counter in column ADCs typically has a constant step size, resulting in linear quantization of the input signal. Since we aim to simulate the impact of quantization on end-images—not to develop a circuit model of the ADC—it is valid to simply view the ADC as a transfer function of electrons to codes. Modeling, therefore, entails scaling pixel electron values into an appropriate code-range set by the resolution of the ADC by appropriately scaling and quantizing.

IX. Noise Model: Overview and Application

A. Model Structure

Each of the individual noise sources is modeled using a separate MATLAB function, and so, they can be linked using a modular approach in order to produce a comprehensive simulation tool. This allows the sensor chain to be modeled in a physically realistic manner and enables the user to choose which noise components to simulate. At the outset, the user must specify the input parameters for the perfect image and the submodules. The code can then be executed, and the simulator works through the imager pipeline, modeling each of the chosen noise components. This produces the desired number of noisy output frames (more than one frame is necessary for simulating video sequences) and a report summarizing the simulation. In terms of processing time, a two-megapixel output frame required several minutes using a desktop PC (depending on scene content and algorithm settings), meaning that video sequences could be simulated in a matter of hours.

B. Model Overview

Fig. 8 shows a block diagram for our complete noise model, along with a list of the user-controllable input parameters for each module. The diagram also indicates whether the stages represent fixed-pattern or temporal components. As discussed earlier, the modular nature of the tool makes it trivial for the user to select which sources of noise to simulate in any given experiment.

C. Sample Application: Dark-Current Couplets

Digital-signal processing can reduce the effect of white pixels caused by dark current. However, if two adjacent pixels are white, then a couplet results, and the processing may have difficulty performing (the high value in each pixel seems more reasonable given that its neighbor is of similar value). Unfortunately, to the observer, these white pixels are highly disturbing. These dark-current couplets are expected to be seen more as image resolution increases.

It is, therefore, useful to compare the noise performance between different resolutions when zoomed into a region of interest in the scene, as demonstrated in Fig. 9. This experiment reveals the expected tradeoff between couplets and resolution and the difficulty in correcting them. Our tool can be used in evaluating the effectiveness of defect-correction and noise-reduction algorithms, which, in the future, will aim to tackle dark-current couplets.

D. Sample Application: VFPN Analysis

Image quality is considerably degraded by the presence of VFPN, even though the standard-deviation value may appear low. Hence, it is interesting to investigate at what level VFPN

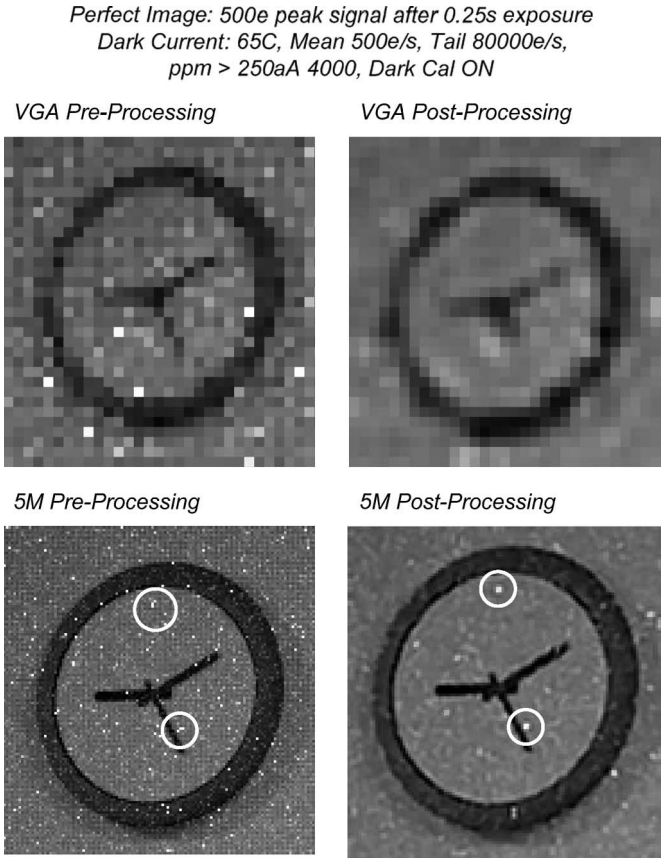

Fig. 9. Effect of dark current on zoomed images at different resolutions. White circles indicate couplets. Note that, for illustration purposes, the noise values chosen represent a worst case example of dark-current performance.

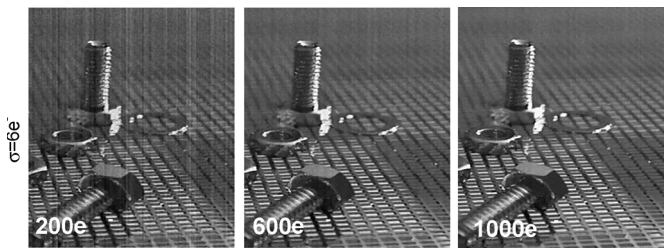

Fig. 10. Images showing the impact of VFPN levels at different light levels.

becomes noticeable in still images at low to medium light, and our noise model offers a straightforward means of carrying out such an investigation. Since photon shot noise influences the degree to which the signal-dependent VFPN is perceptible, it is necessary to include both sources of noise in the simulation.

Fig. 10 shows results from an experiment designed to demonstrate the impact VFPN levels at different light levels. From the images, it is clear that even a very low σ_{VFPN} of six electrons is noticeable in low light, whereas at higher light levels, it is much more difficult to perceive.

E. Realistic End-Image

A sample synthetic image incorporating all of the modeled noises is provided in Fig. 11. Although the parameter values chosen for this example are arguably rather extreme, the tool has been shown to produce realistic-looking output images.

Fig. 11. Simulation of the entire sensor-noise chain, based on exaggerated noise values for illustration purposes.

X. Conclusion

A tool capable of accurately simulating CMOS image-sensor noise and its effect on images has been presented. In particular, we have demonstrated a novel approach in modeling dark current and temporal noise using more representative distributions than some previously published attempts [2], [3]. This leads to a realistic and practical simulation tool. Our noise model has been applied in industry to visualize the likely effect that the proposed process changes will have on output images. This has helped imager designers to decide upon, and justify, targets for new process parameters.

Nonetheless, there is much scope for extension. In particular, a more sophisticated means of modeling RTS and flicker noise is desirable. This would likely require more fundamental research in the field. Furthermore, the complete imaging chain could be simulated by also incorporating optical effects. Work is currently underway in pursuit of this goal, which can be accomplished either by developing appropriate submodules in our existing model or by linking the sensor model with an external optics model.

References

[1] J. Farrell, F. Xiao, P. Catrysse, and B. Wandell, "A simulation tool for evaluating digital camera image quality," *Proc. SPIE*, vol. 5294, pp. 124–131, Dec. 2004.

[2] H. Wach and E. Dowski, "Noise modeling for design and simulation of computational imaging systems," in *Proc. Color Imag. Conf.: Color Sci., Syst., and Appl., Final Program and Proc. IS and T and SID*, 2004, pp. 211–216.

[3] T. Kolehmainen, J. Aikio, M. Karppinen, A. Mattila, J. Makinen, K. Kataja, K. Tukkiniemi, and P. Karioja, "Simulation of imaging system's performance," *Proc. SPIE*, vol. 5178, pp. 204–212, Jan. 2004.

[4] R. Costantini and S. Süsstrunk, "Virtual sensor design," *Proc. SPIE*, vol. 5301, pp. 408–419, Jun. 2004.

[5] A. Theuwissen, "The effect of shrinking pixels in existing CMOS technologies," in *Proc. Fraunhofer IMS Workshop CMOS Imag.*, 2002, pp. 14–30.

[6] L. Grant, "Characterisation of noise sources in CMOS image sensors," presented at the IEEE Solid-State Circuits Conf. Image Sensor Design Forum, San Francisco, CA, Feb. 2005.

[7] R. Henderson and J. Hurwitz, "CMOS image sensor design," presented at the IEEE Custom Integrated Circuits Conf. Workshop, San Diego, CA, May 2001.

[8] K. Findlater, R. Henderson, D. Baxter, J. E. D. Hurwitz, L. Grant, Y. Cazaux, F. Roy, D. Herault, and Y. Marcellier, "SXGA pinned

photodiode CMOS image sensor in 0.35 μm technology," in *Proc. IEEE Int. Solid-State Circuits Conf.*, Feb. 2003, vol. XLVI, pp. 218–219.
[9] Wikipedia Encyclopaedia, *Ray Tracing*, Aug. 2005. [Online]. Available: http://en.wikipedia.org/wiki/Ray_tracing
[10] B. Bayer, "Color imaging array," U.S. Patent 3 971 065, Jul. 20, 1976.
[11] A. Theuwissen, *Solid State Imaging With Charge Coupled Devices*. Boston, MA: Kluwer, 1995.
[12] S. D. Poisson, "Recherches sur la probabilité des jugements en matière criminelle et en matière civile," in *Précédées des Regles Générales du Calcul des Probabilités*. Paris, France: Bachelier, Imprimeur-Libraire pour les Mathematiques, 1837.
[13] W. Mendenhall and T. Sincich, *Statistics for Engineering and the Sciences*, 4th ed. New York: Macmillan, 1994.
[14] H. Rhodes, G. Agranov, C. Hong, U. Boettiger, R. Mauritzson, R. J. Ladd, I. Karasev, J. McKee, E. Jenkins, W. Quuinlin, I. Patrick, J. Li, X. Fan, R. Panicacci, S. Smith, C. Mouli, and J. Bruce, "CMOS imager technology shrinks and image performance," in *Proc. IEEE Workshop Microelectron. and Electron Devices*, 2004, pp. 7–18.
[15] M. Furumiya, H. Ohkubo, Y. Muramatsu, S. Kurosawa, F. Okamoto, Y. Fujimoto, and Y. Nakashiba, "High-sensitivity and no-crosstalk pixel technology for embedded CMOS image sensor," *IEEE Trans. Electron Devices*, vol. 48, no. 10, pp. 2221–2227, Oct. 2001.
[16] R. W. G. Hunt, *The Reproduction of Colour*, 5th ed. Tolworth, U.K.: Fountain Press, 1995.
[17] J. Adams, K. Parulski, and K. Spaulding, "Colour processing in digital cameras," *IEEE Micro*, vol. 18, no. 6, pp. 20–30, Nov./Dec. 1998.
[18] M. Mancuso, "White balancing," presented at the IEEE Solid State Circuits Conf. Image Sensor Design Forum, San Francisco, CA, Feb. 2006.
[19] Kodak Image Sensor Solutions, *CCD Image Sensor Noise Sources*, Jan. 10, 2005. Application Note, Revision 2.1.
[20] J. Janesick, *Scientific Charge-Coupled Devices*. Bellingham, WA: SPIE Press, 2001.
[21] H. L. Peek, D. W. E. Verbugt, and H. Heijns, "A low dark current double membrane poly-Si FT-technology for 2/3 inch 6 M pixel CCD imagers," in *IEDM Tech. Dig.*, Dec. 5–8, 1999, pp. 871–874.
[22] D. Sackett, "CMOS pixel device physics," presented at the IEEE Solid State Circuits Conf. Image Sensor Design Forum, San Francisco, CA, Feb. 2005.
[23] A. W. F. Edwards, *Likelihood: An Account of the Statistical Concept of Likelihood and Its Application to Scientific Inference*. Baltimore, MD: The Johns Hopkins Univ. Press, 1992.
[24] R. Royall, *Statistical Evidence: A Likelihood Paradigm*. London, U.K.: Chapman & Hall, 1997.
[25] N. Balakrishnan, *Handbook of the Logistic Distribution*. New York: Marcel Dekker, 1992.
[26] E. Weisstein, *Inverse Gaussian Distribution*, Oct. 2005. [Online]. Available: http://mathworld.wolfram.com/InverseGaussianDistribution.html
[27] E. L. Crow and K. Shimizu, *Lognormal Distributions: Theory and Applications*. New York: Marcel Dekker, 1988.
[28] C. Leyris, A. Hoffmann, M. Valenza, J.-C. Vildeuil, and F. Roy, "Trap competition inducing R.T.S. noise in saturation range in N-MOSFET," *Proc. SPIE*, vol. 5844, pp. 41–51, May 2005.
[29] J. Scofield, N. Borland, and D. Fleetwood, "Random telegraph signals in small gate area PMOS transistors," in *Proc. Amer. Inst. Phys. Conf.*, 1993, vol. 285, pp. 386–389.
[30] L. K. J. Vandamme and G. Trefan, "Low frequency noise ($1/f$ and RTS) in sub-micron MOSFETs," presented at the Semiconductor Advances Future Electronics (SAFE), Veldhoven, The Netherlands, 2001.
[31] J. S. Kolhatkar, C. Salm, and H. Wallinga, "Separation of random telegraph signals from $1/f$ noise in MOSFETs under constant and switched bias conditions," in *Proc. 33rd IEEE Conf. Eur. Solid-State Device Res.*, 2003, pp. 549–552.
[32] T. Antal, M. Droz, G. Gyorgyi, and Z. Racz, "$1/f$ noise and extreme value statistics," *Phys. Rev. Lett.*, vol. 87, no. 24, pp. 240 601.1–240 601.4, Dec. 10, 2001.
[33] R. A. Fisher and L. H. C. Tippet, "Limiting forms of the frequency distribution of the largest or smallest member of a sample," *Proc. Camb. Philos. Soc.*, vol. 24, pt. 2, pp. 180–190, 1928.
[34] E. J. Gumbel, *Statistics of Extremes*. New York: Columbia Univ. Press, 1958.
[35] J. Beirlant, Y. Goegebeur, J. Segers, and J. Teugels, *Statistics of Extremes: Theory and Applications*. Hoboken, NJ: Wiley, 2004.
[36] T. Sugiki, S. Ohsawa, H. Miura, M. Sasaki, N. Nakamura, I. Inoue, M. Hoshino, Y. Tomizawa, and T. Arakawa, "A 60 mW 10b CMOS image sensor with column-to-column FPN reduction," in *Proc. IEEE Int. Solid-State Circuits Conf.*, Feb. 2000, vol. XLIII, pp. 108–109.

Ryan D. Gow was born in Aberdeen, Scotland, in 1983. He received the M.Eng. degree in electronics and electrical engineering from the University of Edinburgh, Edinburgh, U.K., in 2006.

He was sponsored by STMicroelectronics during his M.Eng. and carried out research and development work at their Imaging Division in Edinburgh. He then was with the Faculty of Economics, the Faculty of Mathematics, and currently, the Judge Business School, Cambridge University, Cambridge, U.K., to pursue postgraduate studies.

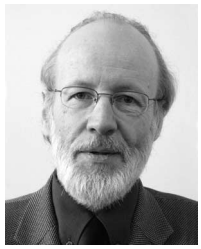

David Renshaw received the B.Sc. degree in pure mathematics, the M.Sc. degree in electronics, and the Ph.D. degree in very large-scale integration (VLSI) design, all in University of Edinburgh, Edinburgh, U.K.

In 1989, a small research team under his direction designed and demonstrated the first single-chip CMOS video camera. In 1990, he was one of three founding members of VLSI Vision Ltd. (VVL), where he worked as a Technical Manager from 1990 to 1995. During that period, VVL grew from a research idea to 80 employees, became the leading supplier of CMOS imager chips and was placed on the London Stock Market. In 1996, he resumed full-time teaching and academic research in the areas of CMOS image sensors, image-sensor processors, image processing applications, and CMOS mixed analog–digital circuits. He continues to encourage and support initial stages of company start-up from these research activities. He is currently a Senior Lecturer in the School of Engineering and Electronics, The University of Edinburgh, where he has been working since 1981. His research interests include VLSI signal processing, analog and digital CMOS circuit design, the design and manufacture of CMOS image sensors, machine vision, and image-processing applications.

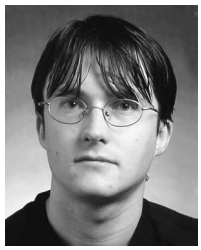

Keith Findlater (S'98–M'01) was born in Edinburgh, U.K., in 1975. He received the M.Eng. and Ph.D. degrees in electronics from the University of Edinburgh, Edinburgh, in 1998 and 2001, respectively.

On completion of his Ph.D., which was industrially sponsored by STMicroelectronics Imaging Division, he was with STMicroeletronics, Edinburgh, as a Technologist. He is currently with Gigle Semiconductor, Edinburgh. His current research interests include circuits, architectures, algorithms, and opto-mechanical systems for advanced camera modules.

Lindsay Grant studied physics at St. Andrews University, St. Andrews, U.K., before embarking on a career in semiconductors.

He has 20 years of experience in semiconductor device physics and process development. He spent 12 years in wafer fabrication, where he held positions in product, device, and process engineering. He has worked on Bipolar, CMOS, DMOS, and BiCMOS technologies. Currently, he works on CMOS technology development for imaging applications. Since 1999, he has been playing a key role in the development and introduction of CMOS image-sensor process technology at STMicroelectronics, Edinburgh, U.K. He has coauthored several imaging papers and was an Invited Speaker at the International Solid-Sate Conference Forum on Image Sensor Characterization.

Stuart J. McLeod received the B.A. degree (with honors), the M.Eng. degree, and the M.A. degree in general engineering followed by electrical and information sciences from Emmanuel College, Cambridge, U.K.

He is currently a Systems Engineer with the Future Technologies Group in the Imaging Division, STMicroelectronics, Edinburgh, U.K., where he has six years experience as an Engineer in the fields of optical communications, front-end semiconductor design, and imaging.

John Hart received the B.Sc. degree from the University of Glascow, Glascow, U.K.

He is an experienced Electronics Engineer with a career in test and characterization. Since joining STMicroelectronics, Edinburgh, U.K., he has worked in electrooptical characterization of CMOS image sensors covering test chip, product prototypes, and production sensors. He is currently working with the Applications Team in the Imaging Division, STMicrolectronics. He is the coauthor of several papers in imaging technology.

Robert L. Nicol received the B.Eng. degree (with honors) and the Ph.D. degree from the Faculty of Engineering, University of Glasgow, Glasgow, U.K., for the study and fabrication of nanometer-scale single-electron devices.

He is currently an Imager Technologist with the Sensor Technology Group in the Imaging Division, STMicroelectronics, Edinburgh, U.K., where he has 11 years experience in new process and technology research and development within the semiconductor and optoelectronics industries.